THE ULTRAVIOLET SPECTRUM OF THE CRAB NEBULA

KRIS DAVIDSON
Department of Astronomy, University of Minnesota

T. R. GULL, S. P. MARAN, AND T. P. STECHER
Laboratory for Astronomy and Solar Physics, NASA Goddard Space Flight Center

R. A. FESEN
Department of Astronomy, University of Michigan

R. A. PARISE AND C. A. HARVEL
Astronomy Department, Computer Sciences Corporation

M. KAFATOS
Department of Physics, George Mason University

AND

V. L. TRIMBLE
Department of Physics, University of California at Irvine

ABSTRACT

Data from 65 hours of observation of the Crab Nebula with the *International Ultraviolet Explorer* are reported, together with new ground-based spectrophotometry. We have measured the important C IV $\lambda1549$, He II $\lambda1640$, and C III] $\lambda1908$ emission line intensities and placed upper limits on other ultraviolet features for the brightest filamentary region in the nebula. We have also measured some ultraviolet continuum surface brightnesses at two places in the Crab.

The emission lines imply an average ionic abundance ratio $n(C^{+2})/n(O^{+2})$ in the range from 0.4 to 1.5 in the observed gaseous condensations. The elemental abundance ratio of carbon to oxygen is probably in the same range. This range may be narrowed through the use of ionization calculations, but even our simple analysis shows that there is no perceptible excess of carbon, due to presupernova nucleosynthesis, in the observed region.

The large helium abundance, small carbon and oxygen abundances, and presence of a neutron star in the Crab Nebula suggest that the presupernova star had a mass close to 8 $M_\odot$ when it was on the main sequence.

Subject headings: nebulae: abundances — nebulae: Crab Nebula — nebulae: supernova remnants — stars: supernovae — ultraviolet: spectra

I. INTRODUCTION

The Crab Nebula is our most easily observed young supernova remnant. It contains a well-known pulsar, and the nebular mass and chemical composition, though not simple to measure, are more directly observable than for any other supernova remnant. Information derived from ground-based optical observations of the Crab has been reported by Woltjer (1958), Mayall (1962), Scargle (1969), Trimble (1970, 1971), Davidson, Crane, and Chincarini (1974), Kirshner (1974), Chevalier and Gull (1975), Wyckoff and Murray (1977), Miller (1978), Davidson (1978, 1979), and by others cited in these sources, while of course many radio and X-ray studies have also been done.

With so much information available, one might expect the Crab Nebula to be a primary basis for theoretical ideas about at least one type of supernova. In fact the Crab has had surprisingly little impact on supernova theory (see Wheeler 1981). Perhaps theorists have been deterred by the wealth of known details; but, on the other hand, two or three crucial observational uncertainties have made theoretical studies of the Crab precarious. One such uncertainty has been the abundance of carbon, which is practically indeterminate from ground-based data alone. In this paper, we describe ultraviolet spectroscopy of the Crab accomplished with the *International Ultraviolet Explorer* (*IUE*) and a resulting estimate of the carbon abundance. We also mention some other interesting results and make some speculative remarks about the main-sequence mass of the supernova precursor star.

The chemical composition of the Crab is significant because it represents actual star-stuff ejected in the supernova explosion, with only a small admixture of swept-up interstellar gas. Most of the visible nebular

696

material is helium, with a mass of the order of 2 $M_\odot$. There is also some hydrogen, perhaps about 0.5 $M_\odot$, possibly mixed with the helium and certainly not well segregated. This hydrogen may have been within the star when it exploded, or it may have been swept up from a circumstellar envelope, or (less likely) it may be swept-up interstellar material. Among heavier elements, the easiest abundance to estimate is that of oxygen—and no perceptible excess oxygen from presupernova nucleosynthesis is found in the Crab Nebula. Visual-wavelength emission lines indicate that the mass fraction of oxygen in the nebular "filaments" is of the order of 0.3%, significantly *less* than in the Sun or the Orion Nebula. Nitrogen, neon, sulfur, and iron abundances are uncertain but probably not very large. In this situation, carbon is of great importance; some supernova models produce helium-rich ejecta that are rich in carbon but not in other heavy elements. Since carbon unfortunately has no visual-wavelength emission lines which are suitable for abundance determinations in the Crab, we must resort to observations of the ultraviolet C III] $\lambda1908$ and C IV $\lambda1549$ features, using the *IUE*.

The surface brightness of the Crab is not high, and a considerable amount of interstellar extinction is present in the ultraviolet; moreover, the angular acceptance of each *IUE* spectrograph aperture includes only a small part of the nebula. Thus the observations reported here were very near the limit of the *IUE*'s capability. (No other young supernova remnant, composed of ejected material, is bright enough to be observed with *IUE*.) We have combined a number of long, faint exposures, in a nontrivial manner, using computer programs developed at Goddard Space Flight Center specifically for the present work. New ground-based spectrophotometry, obtained at the McGraw-Hill Observatory and appropriate for comparison with the *IUE* data, is also reported here.

Our *IUE* observations are described in § II, the data reduction procedures in § III, and the emission line results (along with the ground-based measurements) in § IV. Continuum spectra are briefly discussed in § V. In § VI we discuss the carbon abundance and comment upon the implications for theoretical models of the Crab supernova event and the star that was involved in it.

II. THE OBSERVATIONS WITH *IUE*

The *IUE* is equipped with two spectrographs: long wavelength, 1850—3300 Å, and short wavelength, 1150—1950 Å. Each spectrograph has a large entrance aperture which measures about $10'' \times 20''$ projected on the sky. We used these apertures to examine particular regions in the Crab Nebula, concentrating on the brightest filamentary structures. Preliminary observations of several places in the nebula were made in 1979 August (Davidson *et al.* 1981). More intensive observations of just two regions, chosen according to the 1979
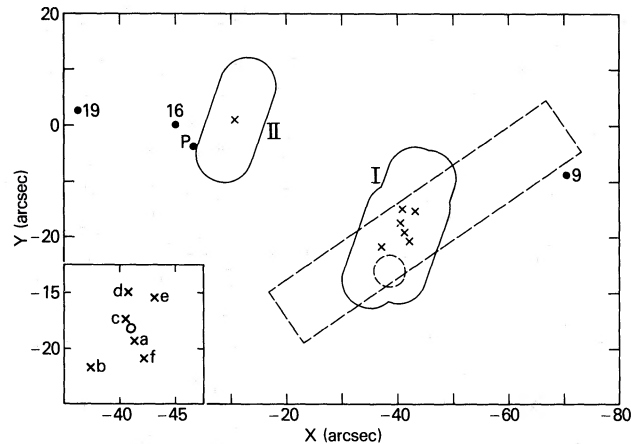

FIG. 1.—Positions of the short-wavelength *IUE* observations; corresponding long-wavelength positions were almost the same. North is upward and east is to the left. "P" marks the Crab pulsar, while "9," "16," and "19" are stars listed by Wyckoff and Murray (1977). The large, oblique, dashed rectangle is Miller's (1978) "position 2," and the small, dashed circle is Davidson's (1978) "bright filament" position. The oblong shapes roughly indicate the size and orientation of the *IUE* large entrance aperture; the $\times$ mark the *IUE* central positions. The insert (*lower left*) is a magnified diagram of the individual positions within Region I.

results, were made in 1980 August[1]. Only the 1980 observations are discussed in this paper.

The places observed in 1980 are shown in Figure 1. Here, the rectangular coordinates (X, Y) are those used by Trimble (1968) and by Wyckoff and Murray (1977). The coordinate X increases eastward, Y increases northward, and $X = Y = 0$ at the star $5''$ northeast of the pulsar NP 0532, i.e., at $\alpha = 5^h 31^m 31^s.6$, $\delta = +21°58'58''$ (equinox 1950). Our "Region I" includes six positions, Ia–If, which do not exactly coincide, because we wished to broaden the spatial coverage by a few arc seconds. The *relative* positions Ia–If, at which short-wavelength spectrograph observations were made, were estimated by reference to three stars detected with the *IUE* Fine Error Sensor, a white-light slit jaw camera. The rms discrepancy between intended and measured relative positions was $1''.2$. The *absolute* positions are less certain. The telescope was usually pointed by offsetting from the star AGK3 $+22°$ 545, located north of the nebula at $5^h 31^m 41^s.5, +22°08'38''$ (1950). In order to check the accuracy of the offset procedure, position Ic was reached by offsetting from a star to the south, near $5^h 31^m 14^s.0$, $+21°52'11''$, aiming for position Ia. The

[1]August is of course an unfavorable month for ground-based observations of the Crab, which is then in a direction only about 50° from the Sun. But this was a preferable pointing direction for the *IUE*, in order to keep an on-board computer from being overheated by direct solar illumination of the "rear" part of the spacecraft.

absolute pointing accuracy should thus be comparable to the measured difference between Ia and Ic, which is less than 3″. As explained in § IV, there is weak evidence for a systematic pointing error of several arc seconds; actual positions may have been south of those indicated in Figure 1.

The oblong large entrance apertures of the spectrographs were oriented with their long axes near position angle 160°, i.e., NNW–SSE. According to R. Panek (1981, private communication), tests show that the angular area accepted by each aperture is nearly 205 arcsec^2 with a formal uncertainty of 3% (although systematic uncertainties may be larger). Observations with each spectrograph were made with the corresponding low-dispersion camera; the 10″ aperture width corresponded to a wavelength interval of about 11 Å in the short-wavelength spectra and 18 Å in the long-wavelength spectra.

Our "Region I," 40″ WSW of the pulsar, includes the brightest filamentary emission line structure in the nebula.[2] We obtained one short-wavelength (1250–1950 Å) and one long-wavelength (2000–3200 Å) spectrum at each of the six positions Ia–If (although the long-wavelength positions may not coincide precisely with those shown in Figure 1). Total integration times of 31 and 17 hours, respectively, were devoted to these short-wavelength and long-wavelength observations. With such a faint object, the individual exposures were expected to produce low-quality spectra; our intent was to combine the data as described in § III below.

Region II, immediately NW of the pulsar, is essentially a nonthermal continuum source with negligible emission lines. It includes some of the "wisps" associated with the pulsar. We obtained two short-wavelength spectra and two long-wavelength spectra of Region II, with total integration times of 9 hours and 8 hours respectively.

As an aid to future users of the *IUE* data, a list of individual exposures is given in Table 1. The data are available from the National Space Science Data Center at Goddard Space Flight Center.

III. DATA REDUCTION

The C IV λ1549, He II λ1640, and C III] λ1908 emission lines were indeed detected in each of our six individual short-wavelength spectra of Region I; but there were also other apparent features of comparable strength, produced by occasional particle-radiation "hits" on the detector and by defective detector pixels. By comparing the spectra with each other, we can determine which features (bright spots or streaks in the

[2] In the 1979 observations (Davidson *et al.* 1981), only one other region in the Crab was found where the emission lines were measurable with the *IUE*. That region, fainter than Region I, is located near $X = +30″$, $Y = -63″$.

TABLE 1

JOURNAL OF *International Ultraviolet Explorer* OBSERVATIONS

Observation Number	Date (1980, UT)	Position	Integration Time (minutes)
SWP 9765	Aug 11	Ia	360
LWR 8485......	Aug 11	Ia	150
SWP 9770	Aug 12	Ib	270
LWR 8491......	Aug 12	Ib	129
SWP 9775	Aug 13	Ic	330
LWR 8495......	Aug 13	Ic	240
LWR 8496......	Aug 13	II	276
SWP 9795	Aug 15	Id	300
LWR 8511......	Aug 15	Id	150
SWP 9796	Aug 15	II	210
LWR 8513......	Aug 15	II	208
SWP 9804	Aug 16	Ie	300
LWR 8519......	Aug 16	Ie	135
SWP 9838	Aug 19	If	300
LWR 8551......	Aug 19	If	210
SWP 9840	Aug 19	II	352

NOTE.—"SWP" denotes a short-wavelength, large-aperture exposure; "LWR" denotes a long-wavelength, large-aperture exposure.

spectral images) are due to radiation hits. By comparing our spectra with other *IUE* spectra—especially "blank field" spectra—we can identify certain bright spots which are semipermanent and unrelated to the object being observed. Some of these "hot pixels" in the detector are known to have existed since the *IUE* was launched, but their physical nature is not well understood. (Each hot pixel does respond to the spectral signal, but also has an extra apparent intensity superposed.) At least one permanent reseau mark, a dark rather than bright feature, also is superposed on each spectrum.

Evidently, given the presence of such strong but localized defects, we must combine the individual exposures very carefully. A simple average of several exposures is inadequate because vestiges of all the radiation hits, as well as undiminished contributions from the permanent bright pixels, remain in such an average—and these can be nearly as strong as the faint, genuine spectral features discussed later in this paper. A median of several exposures, although it retains the permanent defects, is useful because it eliminates radiation hits. We experienced some practical difficulties in attempting to generate simple, pixel-by-pixel, average and median spectra; in particular, the spectral format sometimes moved in position by several pixel widths between exposures, probably because of thermal effects in the spectrograph or detector.

We adopted the following procedure for combining spectral images:

1. Scale the data from each observation to a common equivalent exposure time. Since the actual exposure times for each camera were all rather similar, there is no

need to assign different weights to individual observations.

2. Adjust positions within the spectral images to a common spectral grid. (This is to allow for the format movements mentioned above.)

3. Equalize the average background levels by subtracting a constant level from each spectrum.

4. Generate a pixel-by-pixel average image.

5. Generate a pixel-by-pixel median image.

Results of this procedure are illustrated in Figures 2–5 (Plates 9–12). (Note that these images have not been corrected for the wavelength-dependent instrumental sensitivity.) The six short-wavelength spectral images of Region I are shown in Figure 2, labeled 1A–1F. Each of these shows a continuum, the λ1549, λ1640, and λ1908 emission lines, and various radiation hits and "hot pixels." One particularly strong radiation hit appears near 1850 Å in spectrum F. The average of the six spectra, also shown in Figure 2, has an improved overall signal-to-noise ratio but also includes contributions from all of the radiation hits. The median image, as shown in Figure 2, is slightly better because it is practically free of radiation hits. Figure 3 shows long-wavelength spectral images in the same manner; these have a stronger continuum in the 2500–3200 Å region because the detector sensitivity is higher and interstellar extinction is smaller at such wavelengths, but no emission lines are detected in this spectral region.

Permanent bright spots were difficult to remove from the data. Partial removal was achieved through the use of a median of many *blank-field IUE* spectra. Observing time was of course too valuable to allow long exposures on blank fields as a specific observing project. However, it is possible to operate both *IUE* spectrographs simultaneously, with both large apertures open; therefore, one can obtain a blank-field exposure with one spectrograph while the other is being used to observe some object. Various quasars and distant galaxies were observed with 3–15 hour *IUE* exposures during 1979–1980, and these objects contribute negligible intensities in the complementary large aperture about an arc minute away. Thus, a group of blank-field exposures were obtained with a total exposure time comparable to our total "Region I" Crab Nebula exposure time. These were used to produce median "background" or "flatfield" images, practically free of radiation hits, for short and long wavelengths. These images, labeled "flatfield" in Figures 4 and 5, clearly show many "hot pixels." By subtracting "flatfield" from "median" images, we obtained short-wavelength and long-wavelength spectral images in which the effects of "hot pixels" or permanent bright spots were reduced. These images are shown (labeled "median-flatfield") in Figures 4 and 5.

For several reasons, intensities in our "median minus flatfield" spectra may be unreliable at the "hot pixels." (1) The blank-field exposures were obtained over an 18 month period, with a variety of spacecraft-Sun attitude angles and temperatures. (2) There are slight mismatches between image formats, as mentioned earlier. (3) We have no assurance that the extra intensity at a hot pixel is a linear function of exposure time. (4) It is conceivable that hot pixels are not really permanent. There is no adequate evidence about most of these possible sources of error. But despite these doubts regarding localized spots in the data, our "median minus flatfield" spectral images seem better in most ways than the median and average spectral images. (An apparent feature near 1800 Å in Figure 4 has an exaggerated prominence there because of the photographic form of display; see Fig. 6, discussed below.)

Having assembled "average," "median," and "median minus flatfield" composite spectra, we extracted intensity information from each, using the following procedure (which resembles the standard *IUE* extended-source extraction process):

1. At each wavelength, sum the data across the spectrum perpendicular to the dispersion, using a 10-pixel-high numerical sampling slit (which fairly matches the longer dimension of the entrance aperture).

2. Similarly extract two background samples at each wavelength, one on each side of the spectrum, in each case using a 10-pixel-high sampling slit centered 12 pixels from the midline of the object spectrum.

3. Average the two background determinations from step (2).

4. Perform a 31 point median filtering operation and two successive 15 point running averages on the background spectrum from step (3), in order to find a smoothed background.

5. Obtain a net spectrum by subtracting the smoothed background from the data given by step (1).

6. Apply a wavelength-dependent absolute flux calibration. (This does not include corrections for interstellar extinction.)

7. Smooth the resulting spectrum by taking a 3 point running average.

The results of this procedure, applied to our short-wavelength and long-wavelength data on Region I in the Crab, are shown in Figures 6 and 7.

IV. THE EMISSION LINES IN REGION I

C IV λ1549, He II λ1640, and C III] λ1908 emission features are evident in the short-wavelength spectra of Region I (Figs. 2, 4, and 6). The apparent central wavelengths are about 5 Å less than laboratory wavelengths—partly because of a radial velocity of about -400 km s^{-1} in the emitting gas (see below) and partly because the center of the spectrograph entrance aperture was typically offset to the east of the most intense emission line region, by perhaps 3″ (this was not intentional, of course). Some spatial and spectral structure is
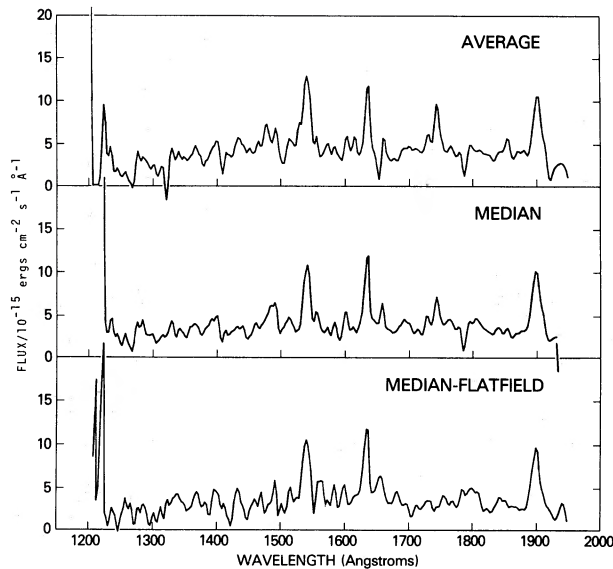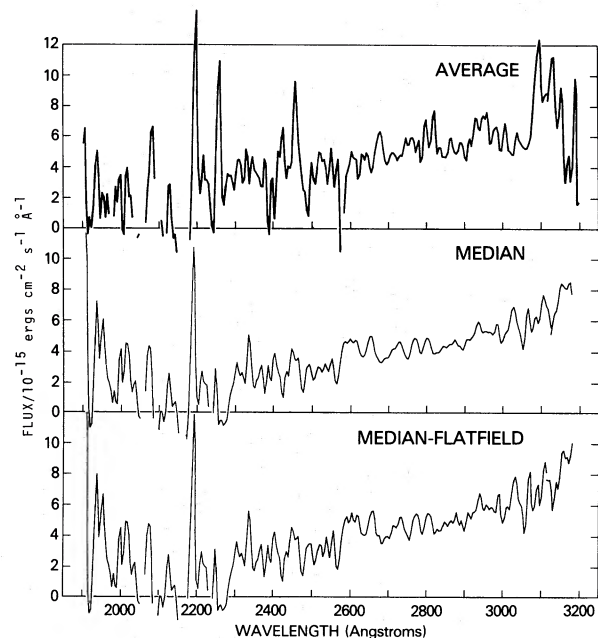
FIG. 6

FIG. 7

FIG. 6.—The average, median, and "median-minus-flatfield" short-wavelength spectra of Region I, corrected for instrumental sensitivity but not for interstellar extinction.

FIG. 7.—The average, median, and "median-minus-flatfield" long-wavelength spectra of Region I, corrected for instrumental sensitivity but not for interstellar extinction. The apparent feature at 2190 Å is an instrumental defect.

present in the emission features in each individual spectral image (see Fig. 2).[3] In the unsmoothed "median" version of the composite spectrum, the line widths at half-maxima are about 13 Å, 6 Å, and 15 Å for λ1549, λ1640, and λ1908 respectively. The corresponding widths at the bases of the lines are 20 Å, 14 Å, and 30 Å. These widths are due to (1) the spatial distribution of the emission, (2) the doublet natures of λ1549 and λ1908, (3) the *IUE* detector resolution, and perhaps (4) a poorer focus for λ1908, near the long-wavelength end of the spectrum.

Ultraviolet line intensities measured in the "average," "median," and "median minus flatfield" composite spectra are listed in Table 2. The λ1549/λ1640/λ1908 intensity ratios are roughly similar in each of the six individual short-wavelength spectra, except that λ1549 seems fainter than λ1640 in the spectrum obtained at position Ie. Each error estimate in Table 2 represents the range in derived intensity which results from moving the adopted baseline (continuum) level up or down

[3] In particular, positions Ib and If were definitely south of the brightest emission line sources. It is surprisingly difficult to correlate Figure 1 and Figure 2 with published photographs of the filamentary structure. This is one reason why we are not totally confident of the absolute positional accuracy of our observations, as mentioned in § II above. There may be a systematic error of several arc seconds.

far enough to be almost an upper or lower envelope, respectively, to the adjoining continuum data. Such error estimates should be pessimistic, aside from undetected systematic effects. Although we suspect that the "median" spectrum is best for determining line intensities, the "adopted" values in Table 2 are averages of the "average," "median," and "median minus flatfield" results.

Some upper limits to undetected emission lines are also listed in Table 2. The C II] λ2326, [Ne IV] λ2440, and Mg II λ2798 upper limits are fairly straightforward and are intended to be "3σ or higher" estimates, considering the relevant noise levels. The limit on N III] λ1749, however, is not straightforward. Each of the individual short-wavelength spectra has a sharp bright feature at 1745 Å; but this is due to an obvious "hot pixel" in the detector, located on one side of the spectrum, while there is also a less obvious defect nearby, seen in blank-field exposures. Thus it would be difficult to confirm the presence of any genuine, weak N III] emission. This is unfortunate, because nitrogen might conceivably be overabundant in the Crab, and most of the nitrogen might be N^{+2}, which has no detectable visual-wavelength lines, rather than N^+, which can be observed from the ground through [N II] λλ6548,6583 emission. The limit on N III] λ1749 given in Table 2 was estimated from (1) the "median minus flatfield" spec-

TABLE 2

OBSERVED ULTRAVIOLET LINE INTENSITIES IN REGION I

Line	"Average" Spectrum	"Median" Spectrum	"Median minus Flatfield"	Adopted
C IV λ1549	92±20	85±20	96±25	90
He II λ1640......	75±15	77±15	90±20	80
N III] λ1749......	...	...	<30:	<30
C III] λ1908......	101±15	108±15	98±20	100
C II] λ2326	...	<75:	<75:	<75
[Ne IV] λ2440 ...	...	<75:	<75:	<75
Mg II λ2798	...	<50	<50	<50

NOTE.—Intensities are given in units of 10^{-15} ergs cm^{-2} s^{-1} passing through the spectrograph entrance aperture. No corrections for interstellar extinction have been applied.

trum and (2) data from just part of the spectrograph entrance aperture, corresponding to a location on the detector that was unaffected by the defects.

Limits on a few other emission lines, such as O III] λ1665 and [O II] λ2470, are omitted from Table 2, because visual-wavelength data allow rough predictions of their intensities which are far below our detection capability. (Incidentally, there was a hot pixel as well as a reseau mark near the λ1665 location.) Regarding possible unanticipated emission lines, all apparent spectral features, other than λ1549, λ1640, and λ1908, coincide with instrumental defects. The one possible exception is a weak feature near 1805 Å, located *between* a reseau mark and a "hot pixel." If this feature is real (which seems unlikely), it has less than half the intensity of He II λ1640.

New ground-based visual-wavelength observations, for comparison with the *IUE* data, were obtained by one of us (R. A. F.) in 1980 November, using a spectral scanner on the 52 inch (1.3 m) McGraw-Hill Telescope on Kitt Peak. Spectra in the 3600–5100 Å and 3600–7000 Å wavelength ranges were obtained, with respective integration times of 20 minutes and 30 minutes and with respective spectral resolutions of about 6 Å and 10 Å. It would have been extremely difficult to obtain data with precisely the same spatial coverage as the *IUE* data; but since relative line intensities are much more uniform than absolute intensities, an approximate sample of Region I was judged adequate. For the 3600–5100 Å spectrum, a 5.6″×20″ slit was oriented N–S and was moved slightly E–W during the exposure. The other spectrum was obtained with a 2″×10″, E–W slit, moved N–S across about 20″ during the exposure. In each case, the average position was near the center of Region I. The data were reduced and corrected for atmospheric extinction and sky brightness in a conventional manner. The overlapping wavelength regions of the two spectra are mutually consistent within reasonable error estimates.

The results of these new ground-based observations are consistent with previous observations of places near Region I, reported by Woltjer (1958), Davidson and Humphreys (1976), Davidson (1978), and Miller (1978). Most of the emission occurs near a radial velocity of −400 km s^{-1} or −500 km s^{-1}, but there are weaker components with other velocities, especially near +800 km s^{-1}. The −400 km s^{-1} component is perhaps 5 times as intense as the +800 km s^{-1} component. In this paper, we list and use the visual-wavelength line intensities in just the major component; but the line ratios would not be changed significantly if the minor components were included. Some lines are uncertain because they include corrections for minor components of nearby lines; in particular, [O III] λ4363 almost coincides with the minor component of Hγ λ4340.

Observed relative intensities of ultraviolet and visual-wavelength emission lines, in and around Region I, are listed in Table 3. Here we have used the He II recombination lines as a link between ground-based and *IUE* data; the intrinsic He II λ1640/λ4686 intensity ratio is assumed to be 7 (Seaton 1978). To correct for interstellar reddening, we adopt $E_{B-V}=0.5$ mag (Miller 1973) along with the ultraviolet extinction estimates by Wu (1981). Table 3 includes some data for places near Region I, quoted from earlier work: Davidson (1978) measured a small area within Region I; "position 2" of Miller (1978) is a large rectangular area which includes Region I; and Miller's (1978) "position 2'" is a small area at the center of the large rectangle (see Fig. 1). For comparison, Table 3 also includes the spectrum of the high-excitation planetary nebula NGC 7662, as observed by Bohlin, Harrington, and Stecher (1978), whose ultraviolet data were obtained with a rocket-borne spectrometer rather than with the *IUE*. The implications of Table 3 are discussed in § VI.

Absolute line intensities in Region I are difficult to assess because of spatial irregularities. Let us adopt 10^{-15} ergs cm^{-2} s^{-1} arcsec^{-2} as a convenient unit of

TABLE 3

RELATIVE EMISSION LINE INTENSITIES

LINE	Å	REGION I[a] (This Paper) F	I	"BRIGHT FILAMENT"[b] I	"POSITION 2"[c] I	"POSITION 2'"[c] I	NGC 7662[d] I
C IV	1549	61	600	...	...	...	720
He II......	1640	54	480	...	...	...	300
N III]	1749	<20	<170	...	...	...	<30
C III]......	1908	68	560	...	...	...	560
C II]	2326	<50	<650	...	...	...	<10
[Ne IV] ...	2440	<50	<400	...	...	...	74
Mg II	2798	<35	<110	...	...	...	<25
[O II]......	3727	630	1000	910	1450	1240 45	14
[Ne III] ...	3869	115	172	150	250	200 13	76
[S II]	4071	17:	24:	40:	40:	50:	<1
Hγ	4340	38	48	50	62	45	47
[O III]	4363	12:	15:	20:	18:	13:	16
He I	4471	19	23	30:	27:	37:	3
[Fe III] ...	4658	7:	8:	10:	...	27:	<1
He II......	4686	63	68	70	83	87	44
Hβ	4861	100	100	100	100	100	100
[O III]	4959	364	350	340	530 }	1720	{ 400
[O III]	5007	1170	1100	1000	1560 }		{ 1150
He I	5876	107	74	...	90	...	7
[Fe VII] ...	6087	11:	7:	...	...	...	<1
[O I]	6300	157	98	130:	104	...	<1
[O I]	6363	61	36	...	...	...	<1
Hα	6563	505:	298:	290: }	844	{ ...	310
[N II]...... 6548, 6583		680:	396:	330: }		{ ...	8
He I	6678	34:	19:	...	...	...	2
[S II]	6717	284:	161: }	580:	468	...	1
[S II]	6731	336:	190: }				

[a] This paper.
[b] Davidson 1978.
[c] Miller 1978.
[d] Bohlin, Harrington, and Stecher 1978.

NOTE.—F = apparent energy intensity, relative to $F(H\beta) = 100$; I = intrinsic energy intensity, corrected for reddening $E_{B-V} = 0.50$ mag.

apparent surface brightness for an emission feature, observed above the Earth's atmosphere. Davidson, Crane, and Chincarini (1974) estimated a maximum Hβ brightness of 2 units, averaged over an area 5″ across within our Region I. Davidson and Humphreys (1976) estimated 4 units for Hβ in an area 2″ across. These seem roughly consistent with an estimate of 2.5 units, estimated from our new ground-based data for a 10″ × 20″ region (although we might have expected this last estimate to be smaller than the Davidson, Crane, and Chincarini value). According to Table 3, the apparent brightness of He II λ1640 is about half that of Hβ and therefore should be close to 1 unit. But the absolute fluxes listed in Table 2, referring to an area of about 205 arcsec^2, correspond to only about 0.4 unit for He II λ1640. We do not know exactly why this discrepancy

has occurred, but we also do not regard it as a significant mystery; probably some of the *IUE* observations included mostly low-intensity areas. This may be weak evidence for systematic pointing errors as mentioned earlier. Emission line intensities in the Crab Nebula are known to be so irregular that small pointing errors often result in large changes in measured fluxes. The *ratios* of line intensities, as listed in Table 3, are far less dependent upon position.

V. THE NONTHERMAL CONTINUUM

Avoiding some wavelengths where instrumental defects affect the data, we have used the *IUE* spectra to estimate continuum intensities in Regions I and II. These results are plotted in Figure 8. Here we use λI_λ,
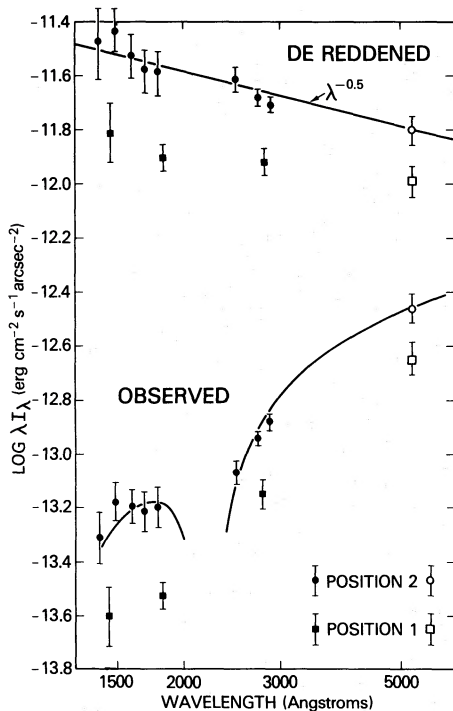
FIG. 8.—Estimated continuum surface brightnesses in Regions I and II.

central $150'' \times 150''$ region in the Crab. Region I appears to have $\lambda I_\lambda \approx \lambda^{-0.2}$ but with a rather large uncertainty in the exponent (± 0.2?). The suspected difference in spectral indices between Regions I and II is qualitatively plausible (see Scargle 1969) and may be real.

The 2200 Å interstellar extinction feature is very pronounced in the lower part of Figure 8. This is one reason why our data are poor in the 2000–2500 Å wavelength region; the other reason is that the *IUE* long-wavelength spectrograph is less sensitive toward shorter wavelengths.

VI. DISCUSSION

Self-consistent ionization calculations will be needed for optimum use of the data in Table 3. However, we can make some interesting estimates without resorting to elaborate calculations. In this section, we first discuss abundance estimates and then comment on the implications for supernova models.

Nebular ionization structure and emission line analyses of the appropriate types have been described by Davidson and Netzer (1979) and by Kafatos and Lynch (1980), and photoionization in the specific case of the Crab Nebula has been discussed by Davidson (1973, 1979). Various other relevant papers are cited by these authors. The gaseous condensations or "filaments" of the Crab are photoionized by the nonthermal continuum of the nebula and are stratified in ionization. (Some extra heating may be due to processes other than photoionization.) Each condensation is thought to have a high-ionization zone near its surface, predominantly a mixture of H^+, He^+, He^{+2}, C^{+2}, C^{+3}, N^{+2}, N^{+3}, O^+, O^{+2}, O^{+3}, etc., at temperatures above 12,000 K. More highly ionized species such as C^{+4} and O^{+4} are probably scarce because the (ionizing radiation)/(electron density) ratio is rather low. If a condensation is thick enough, it also has an inner, low-ionization zone of H^+, He^0, C^+, C^{+2}(?), N^+, O^+, etc., at temperatures below 10,000 K. A very thick condensation may have a yet lower ionization core, mainly H^0, He^0, C^+, N^0, O^0, etc., heated by X-rays. All of these zones exist, irresolvably, in various condensations within our Region I. Our present estimate of the [O III] $\lambda 4363/(\lambda\lambda 4959, 5007)$ intensity ratio in Region I (see Table 3) implies $T_{\text{[O III]}} \approx 12,700$ K, somewhat lower than average for [O III] zones in the Crab Nebula. The [S II] $\lambda 4071/\lambda 6724$ ratio gives $T_{\text{[S II]}} \approx 8000$ K, a typical value, for the low-ionization zones in Region I, while the [S II] $\lambda 6731/\lambda 6716$ ratio indicates that electron densities are of the order of 10^3 cm^{-3} in those zones. These and other visual-wavelength emission lines observed in Region I yield results consistent with previous work on the Crab: the oxygen/hydrogen abundance ratio is roughly "solar," but since most of the mass is helium rather than hydrogen, the mass fraction of oxygen is therefore less than the solar value. Nitrogen, neon, sulfur, and iron

which is the same as νI_ν and which can be expressed in ergs cm^{-2} s^{-1} arcsec^{-2}, as the most appropriate measure of continuum surface brightness—partly because λI_λ directly indicates the energy distribution per logarithmic interval (i.e., it shows where most of the energy flux is) and partly because this choice alleviates possible confusion about units of wavelength, frequency, or photon-energy intervals. The bottom half of Figure 8 shows apparent surface brightnesses as observed above the Earth's atmosphere. The visual-wavelength values were estimated from an isophote map given by Davidson, Crane, and Chincarini (1974), but with the intensities reduced by a factor of 0.85 at each isophote for reasons given at the end of that paper. The upper half of Figure 8 shows the same data, corrected for interstellar extinction with the extinction curve adopted by Wu (1981). Wu agrees with Miller (1973) that the reddening is $E_{B-V} = 0.5$ mag.

At visual and ultraviolet wavelengths, the nonthermal continuum of the Crab Nebula makes a transition from $\lambda I_\lambda \approx \lambda^{-0.8}$ (the radio and infrared power law) to $\lambda I_\lambda \approx \lambda^{+0.2}$ (the X-ray spectrum). We might therefore expect some curvature on a log-log plot of the visual-ultraviolet continuum. Nevertheless, power-law approximations as shown in the upper part of Figure 8 are adequate to fit our data. Region II, near the pulsar, has $\lambda I_\lambda \approx \lambda^{-0.5}$, in excellent agreement with the result of Wu (1981) for the

abundances are less straightforward because their relevant ionization fractions must be estimated from self-consistent ionization calculations.

a) Carbon and Nitrogen in the Crab Nebula

The only carbon features in the visual-wavelength spectrum of the Crab are recombination lines such as C II λ4267, which are very faint, unreliable abundance indicators. Evidently the ultraviolet lines are crucial. The *IUE* observations can be used to set limits on the carbon/oxygen abundance ratio.

If O^{+2}, C^{+2}, and C^{+3} are mixed together in a region at temperature T, with electron density n_e of the order of 10^3 cm^{-3}, the intensity ratios of some emitted lines of interest are

$$\frac{I(\text{C III}] \,\lambda1908)}{I([\text{O III}] \,\lambda\lambda4959, 5007)} \approx 10 \frac{n(\text{C}^{+2})}{n(\text{O}^{+2})}$$

$$\times \exp\left(-\frac{46,500 \text{ K}}{T}\right), \quad (1)$$

$$\frac{I(\text{C IV} \,\lambda1549)}{I([\text{O III}] \,\lambda\lambda4959, 5007)} \approx 50 \frac{n(\text{C}^{+3})}{n(\text{O}^{+2})}$$

$$\times \exp\left(-\frac{64,000 \text{ K}}{T}\right). \quad (2)$$

Here we have used collision strengths from Seaton (1975), Taylor *et al.* (1977), and Dufton *et al.* (1978); of course "λ1549" and "λ1908" are really pairs of lines, λλ1548, 1551, and λλ1906, 1909. Because of their strong temperature dependences, the ultraviolet lines should originate in the hotter ionization zones, roughly corresponding to the [O III] emission zones in Region I. If we simply insert the line intensities from Table 3 into equations (1) and (2), assuming $T = T_{[\text{O III}]} = 12,700$ K, we find $n(\text{C}^{+2})/n(\text{O}^{+2}) \approx 1.5$ and $n(\text{C}^{+3})/n(\text{O}^{+2}) \approx 1.3$. The former ratio might be taken as a plausible guess for n_C/n_O because the average ionization fraction $n(\text{C}^{+2})/n_\text{C}$ should not be very different from $n(\text{O}^{+2})/n_\text{O}$ in the relevant zones (although this statement must be verified through self-consistent ionization calculations).

However, a temperature of 12,700 K is probably too low for the present purpose. If there are temperature gradients in the relevant zones (as there probably are), then the ultraviolet lines must arise mostly in gas which is hotter than the observationally defined $T_{[\text{O III}]}$. Moreover, since $T_{[\text{O III}]} = 12,700$ K is lower than average in the Crab Nebula, we suspect that any observational error in this value is more likely to have been downward rather than upward. Therefore, as an extreme example, suppose that we assume $T = 20,000$ K in equation (1);

this is about the maximum value allowed by existing photoionization models. Then we find $n(\text{C}^{+2})/n(\text{O}^{+2}) \approx 0.4$.

In summary, if we make reasonable allowances for uncertainties in the temperatures and ionization fractions, we can estimate that $0.3 \lesssim n_\text{C}/n_\text{O} \lesssim 3$ in Region I; the most likely range is $0.5 \lesssim n_\text{C}/n_\text{O} \lesssim 1.5$. These limits are susceptible to refinement by means of self-consistent ionization calculations. Bohlin, Harrington, and Stecher (1978) have discussed the rather similar case of n_C/n_O in the planetary nebula NGC 7662, whose line intensities are summarized in Table 3.[4]

Our data can also be used to place a worthwhile limit on the nitrogen abundance. From ground-based observations, one can estimate the abundance of N$^+$, and photoionization calculations allow one to guess the average ionization fraction $n(\text{N}^+)/n_\text{N}$. However, this is not quite adequate; N^{+2}, not N$^+$, is the favored ionization state, and it is unwise to place very much trust in the ionization calculations without adequate observational confirmation. N^{+2} is potentially observable through its ultraviolet N III] λ1749 emission. If N^{+2} and C^{+2} are mixed, their line ratio is

$$\frac{I(\text{N III}] \,\lambda1749)}{I(\text{C III}] \,\lambda1908)} \approx 0.4 \frac{n(\text{N}^{+2})}{n(\text{C}^{+2})}$$

$$\times \exp\left(-\frac{6800 \text{ K}}{T}\right). \quad (3)$$

Thus, from the *IUE* data, we estimate that $n(\text{N}^{+2}) < n(\text{C}^{+2})$, which presumably means that there is less nitrogen than carbon in Region I of the Crab Nebula. This is useful (though probably not surprising), since it excludes some very nitrogen-rich scenarios. However, a moderate nitrogen overabundance, compared with the solar composition, is possible.

Our results refer specifically to Region I, a group of bright condensations. Conceivably, some other part of the Crab Nebula might be far richer in carbon (or

---

[4]We should note that our observed C IV λ1549/C III] λ1908 intensity ratio is surprisingly large, in the following sense. If one calculates an equilibrium photoionization model with the ultraviolet radiation density thought to occur in the Crab and with $n_e \approx 10^3$ cm^{-3}, including both radiative and dielectronic recombination and charge transfer reactions, one finds that there·"should be" much less C^{+3} than C^{+2}. A similar problem occurs with the helium lines; the He^{+2}/He$^+$ ratio implied by observed He II/He I recombination line ratios is larger than in simple photoionization calculations (see Davidson 1973). The explanation may involve the electron densities. Measured values of n_e result from [O II] and [S II] line ratios, and therefore refer to zones of low ionization. Higher ionization zones probably occur nearer to the "surfaces" of the nebular condensations, and electron densities may be lower there, allowing higher equilibrium ionization levels. We do not understand the dynamics of the condensations, whose edges may be quite ill defined. This problem requires observations with high spatial resolution, perhaps attainable with the Space Telescope.

nitrogen or oxygen or all three elements), but this seems improbable. Hydrogen and helium are fairly well distributed throughout the nebula (even if their ratio varies from place to place), and there is no evidence from ground-based data for pronounced segregation of chemical elements. If a condensation were extremely rich in carbon, i.e., with carbon accounting for several percent or more of the local mass, the resulting additional cooling by C III] $\lambda1908$ and C IV $\lambda1549$ emission would lower the temperature there. This would cause a measured value of $T_{[O\ III]}$ to be lower in such a region than in Region I, while the [O III] and [Ne III] lines would be weaker, relative to the Balmer recombination lines, than in Region I. However, Region I seems to have one of the *coolest* known values of $T_{[O\ III]}$ in the Crab. This suggests that other condensations are unlikely to be much richer in carbon. If there are some unobserved, cooler, carbon-rich condensations, it seems unlikely that they can account for more than a small fraction of the mass of the nebula. Abundance gradients may occur *within* condensations (a problem requiring investigation with the Space Telescope), but any hypothetical carbon-rich material then must be concentrated in the low-ionization cores of the thickest condensations; this seems implausibly artificial.

Can some carbon-rich material exist as interfilament gas in the Crab Nebula? Such gas must be hot and quite rarified because it produces no perceptible visual-wavelength emission lines and because its pressure must not be too high; therefore, it must fill an appreciable fraction of the observed nebula in order to have much mass. If such a medium exists, its X-ray emission lines must evidently be below present detection limits but may eventually be detectable with higher resolution X-ray spectrometers. The existence of an interfilament plasma in the nebula is also susceptible to test via measurements of changes in the pulsar's dispersion measure (Davidson and Tucker 1970). Pending such tests, there is no evidence for such gas, aside from the non-thermal high-energy particles whose total mass is negligible; and even if such gas exists, there is no definite *a priori* expectation that it is more carbon-rich than the filaments.

Finally, carbon-rich material might reside in an undetected shell of ejecta outside the observed nebula, but this would require a surprising inversion of the radial arrangement of material in the supernova explosion. While acknowledging the above possibilities, we emphasize that the available evidence is *against* overabundances of either carbon or oxygen in the Crab Nebula, while nitrogen cannot be more than moderately overabundant, relative to the "solar" composition.

b) Implications for the Supernova Event

Our main conclusion, that the ratio of carbon to oxygen in the Crab Nebula is near unity, should be considered in relation to supernova models and also in terms of recent ideas about the evolution of supergiants of various masses.

Arnett (1975) proposed two alternative scenarios for the Crab supernova. Although this work may have been superseded by more recent theoretical calculations, it is of interest here because Arnett explicitly addressed the case of the Crab Nebula. In his "Case A," the nebular ejecta included stellar layers down to the oxygen-burning shell; then carbon, oxygen, and neon should be quite overabundant, relative to the solar composition—a prediction contrary to the results of ground-based observations. In Arnett's "Case B," only layers down to the helium-burning shell were ejected; then oxygen and neon would not be overabundant in the nebula, so this case might be consistent with ground-based observations. However, the "Case B" nebular carbon abundance should be large, $n_C/n_O \gtrsim 10$; therefore, our *IUE* observations appear to exclude this model also.

Recent theoretical work on the evolution of massive stars, from main sequence to supernova, suggests the probable mass range in which a Type II supernova occurs *and* a neutron star is formed (Sugimoto and Nomoto 1980; Nomoto 1981). We assume here that neutron stars have masses of about 1.4 $M_\odot$, consistent with observational results on neutron stars in binary systems (Rappaport and Joss 1980). In a star whose main-sequence mass exceeds about 15 $M_\odot$, the supernova explosion is thought to eject matter which has undergone helium burning and which has been processed as far as oxygen; heavier elements are produced in the explosion itself. If one considers stars of successively smaller initial masses, evolutionary models (including stellar wind mass loss) suggest that, at some point, perhaps $M \approx 10$ $M_\odot$, the synthesized oxygen is no longer above the limiting depth for ejection, while carbon-enriched material is still ejected in the supernova event. Proceeding to yet lower masses, stars with initial masses of about 8 $M_\odot$ eject material which is helium rich but not necessarily carbon rich. In these stars, the helium might be mixed with hydrogen in the convective layers above the helium-burning zones. Stars with initial masses slightly less than 8 $M_\odot$ are likely to produce carbon-deflagration supernovae; they are totally disrupted, produce heavy elements in their explosions, and leave no neutron stars. Such a star could not have produced the Crab Nebula pulsar. At still lower masses, of course, planetary nebulae with white dwarfs are produced.

As discussed above, the Crab Nebula is helium rich but apparently not carbon rich; and a neutron star was formed with the nebula. This combination is to be expected from a Type II supernova whose star had a main-sequence mass of about 8 $M_\odot$, if the theoretical ideas summarized above are correct. The visible nebular mass is perhaps 2 $M_\odot$ or 3 $M_\odot$, as mentioned in § I, and the pulsar has perhaps 1.4 $M_\odot$; so, if the initial stellar mass was 8 $M_\odot$, then roughly 4 $M_\odot$ is "missing"—

presumably lost in wind episodes during blue and red supergiant stages (see Conti and McCray 1980) while evolving toward its dramatic fate. The amount of helium enrichment of the interstellar medium by supernovae like the Crab is worth investigating.

Possible effects due to any hypothetical close stellar companion have been neglected in the above discussion, and we have not mentioned the fact that the Crab is rather far from the galactic plane. Also, we have not considered whether the rather small kinetic energy of expansion of the visible nebula is theoretically "reasonable."

REFERENCES

Arnett, W. D. 1975, *Ap. J.*, **195**, 727.
Bohlin, R. C., Harrington, J. P., and Stecher, T. P. 1978, *Ap. J.*, **219**, 575.
Chevalier, R. A., and Gull, T. R. 1975, *Ap. J.*, **200**, 399.
Conti, P. S., and McCray, R. 1980, *Science*, **208**, 9.
Davidson, K. 1973, *Ap. J.*, **186**, 223.
_____. 1978, *Ap. J.*, **220**, 177.
_____. 1979, *Ap. J.*, **228**, 179.
Davidson, K., Crane, P., and Chincarini, G. 1974, *A.J.*, **79**, 791.
Davidson, K., Gull, T. R., Maran, S. P., Stecher, T. P., Kafatos, M., and Trimble, V. L. 1981, in *The Universe at Ultraviolet Wavelengths*, ed. R. D. Chapman (NASA Conference Pub. 2171), p. 693.
Davidson, K., and Humphreys, R. M. 1976, *Pub. A.S.P.*, **88**, 312.
Davidson, K., and Netzer, H. 1979, *Rev. Mod. Phys.*, **51**, 715.
Davidson, K., and Tucker, W. D. 1970, *Ap. J.*, **161**, 437.
Dufton, P. L., Berrington, K. A., Burke, P. G., and Kingston, A. E. 1978, *Astr. Ap.*, **62**, 111.
Kafatos, M., and Lynch, J. P. 1980, *Ap. J. Suppl.*, **42**, 611.
Kirshner, R. P. 1974, *Ap. J.*, **194**, 323.
Mayall, N. U. 1962, *Science*, **137**, 91.

Miller, J. S. 1973, *Ap. J.* (*Letters*), **180**, L83.
_____. 1978, *Ap. J.*, **220**, 490.
Nomoto, K. 1981, in *IAU Symposium 93, Fundamental Problems in the Theory of Stellar Evolution*, ed. D. Sugimoto, D. Q. Lamb, and D. N. Schramm (Dordrecht: Reidel), p. 295.
Rappaport, S., and Joss, P. C. 1980, "Binary X-Ray Pulsars," MIT Report No. CSR-HEA-80-24 (Cambridge, Mass.)
Scargle, J. D. 1969, *Ap. J.*, **156**, 401.
Seaton, M. J. 1975, *M.N.R.A.S.*, **170**, 475.
_____. 1978, *M.N.R.A.S.*, **185**, 5P.
Sugimoto, D., and Nomoto, K. 1980, *Space Sci. Rev.*, **25**, 155.
Taylor, P. O., Gregory, D., Dunn, G. H., Phaneuf, R. A., and Crandall, D. H. 1977, *Phys. Rev. Letters*, **39**, 1256.
Trimble, V. 1968, *A.J.*, **73**, 535.
_____. 1970, *A.J.*, **75**, 926.
_____. 1971, in *IAU Symposium 46, The Crab Nebula*, ed. R. D. Davies and F. G. Smith (Dordrecht: Reidel), p. 12.
Wheeler, J. C. 1981, *Rept. Progr. Phys.*, **44**, 85.
Woltjer, L. 1958, *Bull. Astr. Inst. Netherlands*, **14**, 40.
Wu, C. C. 1981, *Ap. J.*, **245**, 581.
Wyckoff, S., and Murray, C. A. 1977, *M.N.R.A.S.*, **180**, 717.

KRIS DAVIDSON: Astronomy Department, University of Minnesota, 116 Church Street S.E., Minneapolis, MN 55455

ROBERT A. FESEN and THEODORE R. GULL: Code 683, NASA/Goddard Space Flight Center, Greenbelt, MD 20771

CHRISTOPHER A. HARVEL and RONALD A. PARISE: Computer Sciences Corporation, Code 685, NASA/Goddard Space Flight Center, Greenbelt, MD 20771

MINAS KAFATOS: Department of Physics, George Mason University, 4400 University Drive, Fairfax, VA 22030

STEPHEN P. MARAN and THEODORE P. STECHER: Code 680, NASA/Goddard Space Flight Center, Greenbelt, MD 20771

VIRGINIA L. TRIMBLE: Department of Physics, University of California at Irvine, CA 92717
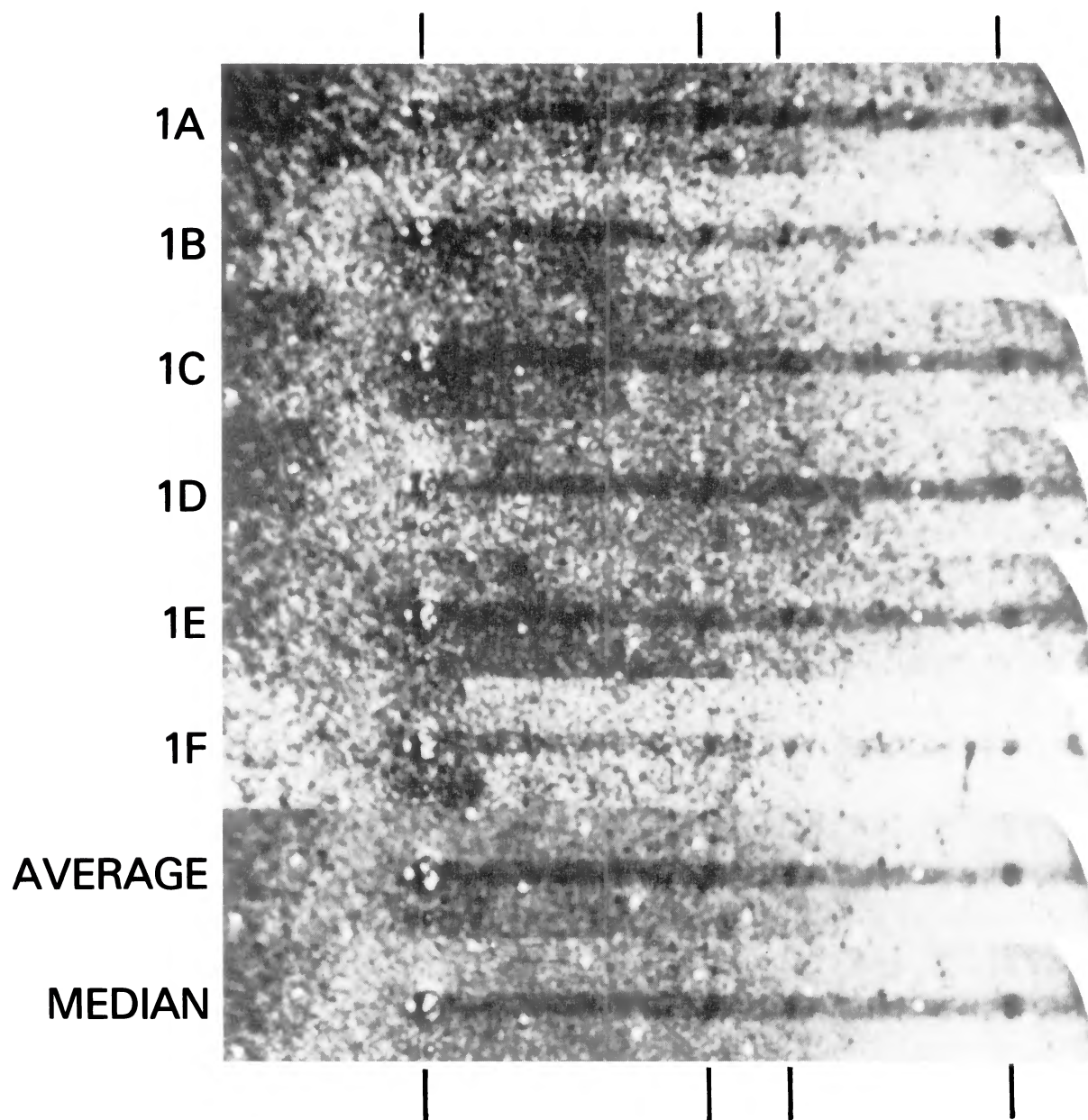
PLATE 9

FIG. 2.—The six individual short-wavelength spectral images of Region I, their average, and their median. These have not been corrected for wavelength-dependent instrumental sensitivity, which is greater toward longer wavelengths (*i.e.*, *to the right*). Vertical marks at top and bottom indicate the wavelengths of (*from left to right*) geocoronal Lα, C IV λ1549, He II λ1640, and C III] λ1908.

DAVIDSON *et al.* (*see* page 699)
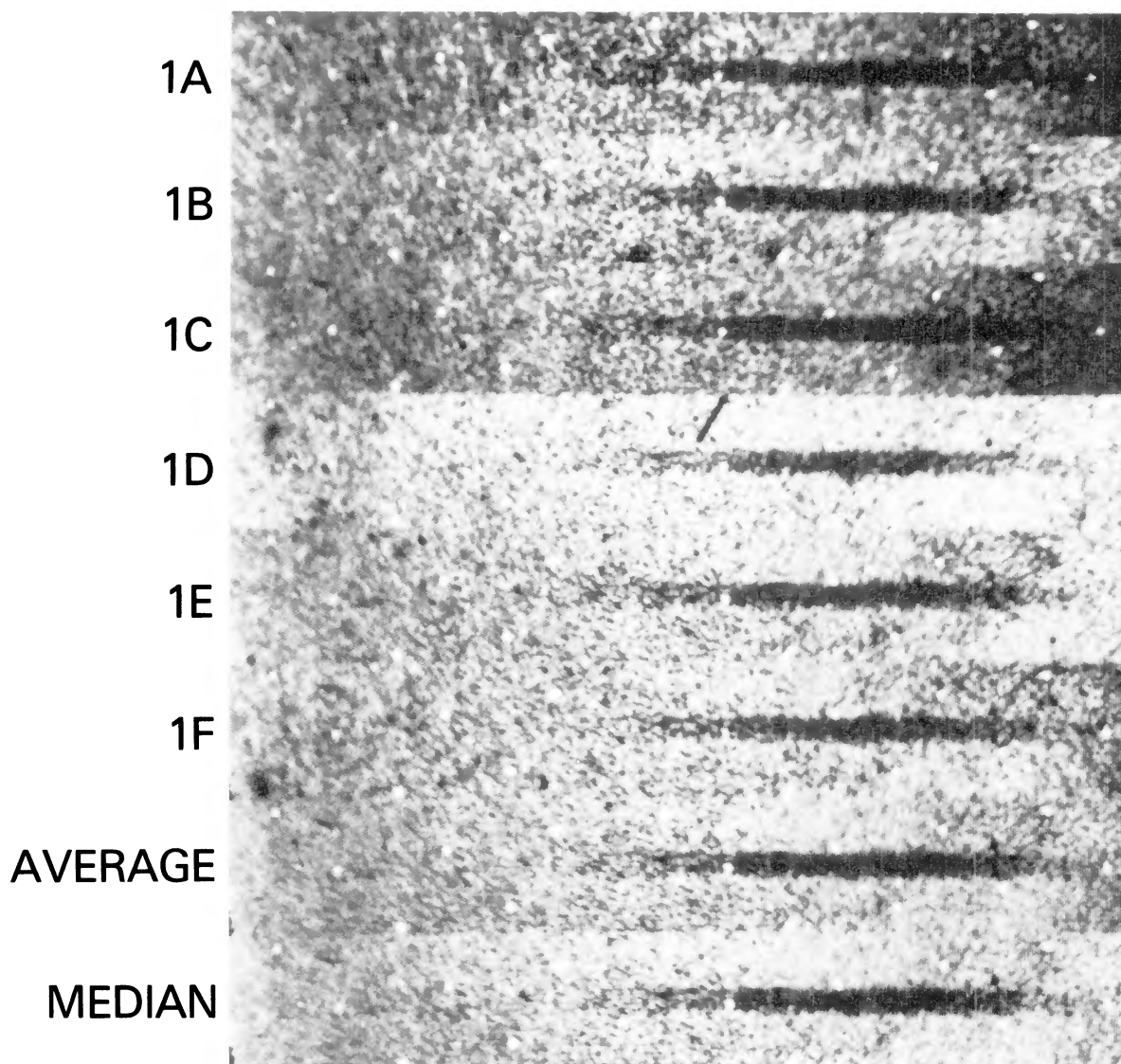
1A

1B

1C

1D

1E

1F

AVERAGE

MEDIAN

FIG. 3.—The six individual long-wavelength spectral images of Region I, their average, and their median. The wavelength range is approximately 2000 Å (*left*) to 3200 Å (*right*). Between 2000 and 2400 Å, the continuum is almost undetectable, because of the 2200 Å interstellar extinction feature and lower instrumental sensitivity at shorter wavelengths.
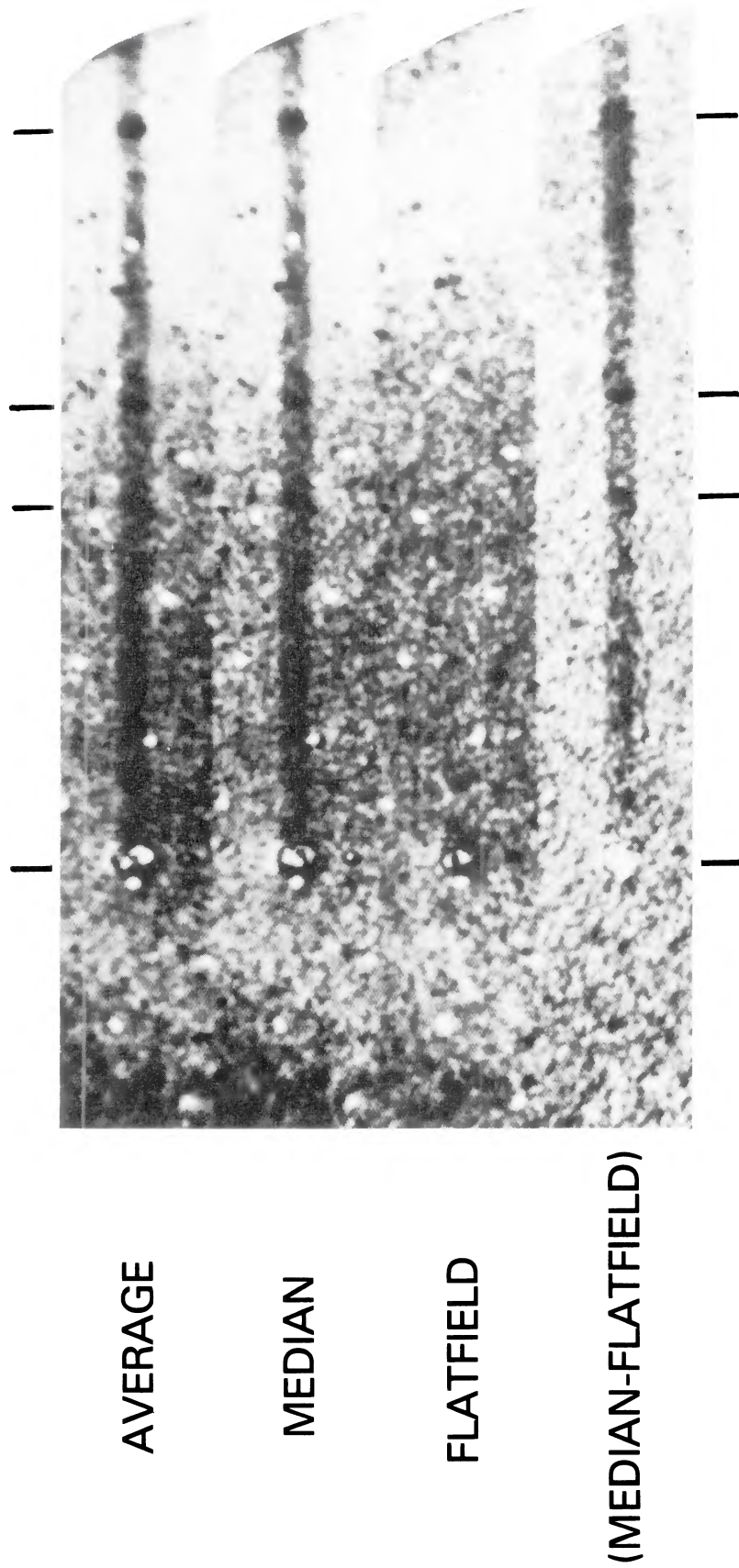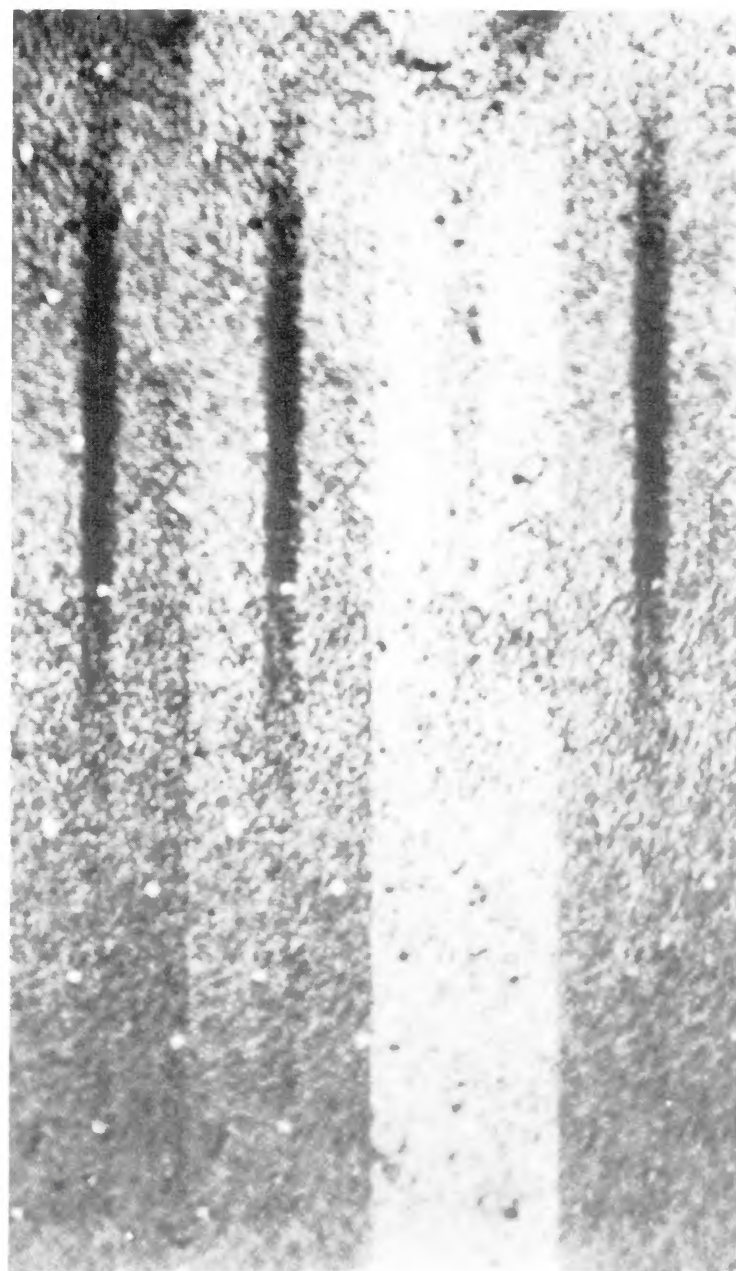
DAVIDSON *et al.* (*see* page 699)

PLATE 11

AVERAGE

MEDIAN

FLATFIELD

(MEDIAN-FLATFIELD)

FIG. 4.—The average, median, and "median-minus-flatfield" short-wavelength spectral images of Region I, displayed as in Fig. 2. In the "median-minus-flatfield" spectrum, an apparent feature near 1800 Å is exaggerated in this form of display; its peak intensity is actually low (*cf.* Fig. 6). The geocoronal Lα feature appears as strong "absorption" feature in the same spectrum because it was saturated in each individual spectrum and various renormalization factors have been applied.

DAVIDSON *et al.* (*see* page 699)

PLATE 12

AVERAGE

MEDIAN

FLATFIELD

(MEDIAN-FLATFIELD)

FIG. 5.—The average, median, and "median-minus-flatfield" long-wavelength spectral images of Region I, displayed as in Fig. 3

DAVIDSON *et al.* (*see* page 699)